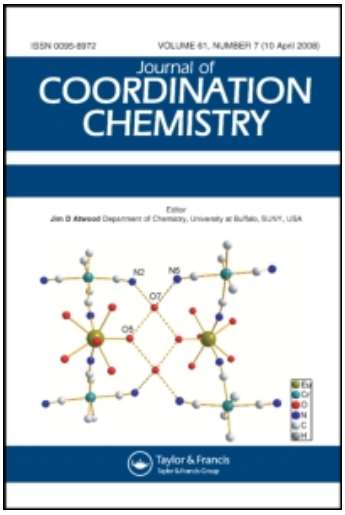

Journal of Coordination Chemistry
Publication details, including instructions for authors and subscription information:
http://www.informaworld.com/smpp/title~content=t713455674

Synthesis and characterization of Schiff base metal complexes: their antimicrobial, genotoxicity and electrochemical properties

Mehmet Tümer[a]; Eyup Akgün[a]; Sevİl Toroğlu[b]; Ahmet Kayraldiz[b]; Lale Dönbak[b]
[a] Chemistry Department, Faculty of Science and Arts, K.Maraş Sütcü Imam University, K.Maras, Turkey [b] Biology Department, Faculty of Science and Arts, K.Maraş Sütcü Imam University, K.Maras, Turkey

First published on: 22 September 2010

To cite this Article Tümer, Mehmet , Akgün, Eyup , Toroğlu, Sevİl , Kayraldiz, Ahmet and Dönbak, Lale(2008) 'Synthesis and characterization of Schiff base metal complexes: their antimicrobial, genotoxicity and electrochemical properties', Journal of Coordination Chemistry, 61: 18, 2935 — 2949, First published on: 22 September 2010 (iFirst)
To link to this Article: DOI: 10.1080/00958970801989902
URL: http://dx.doi.org/10.1080/00958970801989902

Journal of Coordination Chemistry
Vol. 61, No. 18, 20 September 2008, 2935–2949

Taylor & Francis
Taylor & Francis Group

Synthesis and characterization of Schiff base metal complexes: their antimicrobial, genotoxicity and electrochemical properties

MEHMET TÜMER*†, EYUP AKGÜN†, SEVİL TOROĞLU‡, AHMET KAYRALDIZ‡ and LALE DÖNBAK‡

†Chemistry Department, Faculty of Science and Arts, K.MaraŞ Sütcü Imam University, 46100, K.Maras, Turkey
‡Biology Department, Faculty of Science and Arts, K.MaraŞ Sütcü Imam University, 46100, K.Maras, Turkey

(*Received 19 October 2007; in final form 3 December 2007*)

We have synthesized the three Schiff-base ligands H_2L^1–H_2L^3 and their Co^{II}, Fe^{III} and Ru^{III} metal complexes. All compounds have been characterized by analytical and spectroscopic methods. Oxidation of cyclohexane has been done by the metal complexes in CH_3CN using H_2O_2 and/or *t*-butylhydroperoxide (TBHP) as a co-catalyst. The keto-enol tautomeric forms of the ligands have been studied in polar and non-polar organic solvents. Electrochemical properties of the complexes have been studied at different scan rates. Thermal studies were carried out for the compounds. The ligands H_2L^1–H_2L^3 were mutagenic on *Salmonella Typhimurium* TA 98 strain in the presence and/or absence of S9 mix. While the ligands H_2L^1 and H_2L^2 showed mutagenic activity on the strain TA 100 with and without S9 mix, the ligand H_2L^3 was not mutagenic for TA 100. Antimicrobial activity studies of the compounds have also been carried out.

Keywords: Schiff base; Antimicrobial activity; Genotoxicity; Electrochemical

1. Introduction

Schiff bases have played a special role as chelating ligands in main group and transition metal coordination chemistry, due to their stability under a variety of oxidative and reductive conditions and to the fact that imine ligands are borderline between hard and soft Lewis bases [1]. Transition metal complexes of tetradentate Schiff-base ligands find applications in catalysis [2].

Transition-metal complexes catalyze hydrocarbon oxidations [3] by molecular oxygen and/or various oxygen donors, particularly hydrogen peroxide [4]. Selective and partial oxidation of hydrocarbons to oxygen-containing compounds (alcohols, aldehydes, ketones and acids) is extremely important for the chemical industry. Terminally oxidized hydrocarbons are potential feedstocks for the chemical and pharmaceutical industry. However, these reactions represent a challenge because alkanes are relatively unreactive

*Corresponding author. Email: mtumer@ksu.edu.tr

ISSN 0095-8972 print/ISSN 1029-0389 online © 2008 Taylor & Francis
DOI: 10.1080/00958970801989902

due to their high ionization energy, p*K*a values and low electron affinity; in forming oxidation products, their selectivity is usually quite low [5, 6].

Testing of genotoxicity is a preliminary step in safety assessments for newly synthesized pharmaceuticals, food additives, and industrial substances [7–9]. The bacterial Ames test, developed in 1975 [10], is a widely used screening test for the possible genotoxic effects of chemical compounds (the ability to induce mutation or cancer). The assay done in *Salmonella typhimurium* bacteria gives much faster and less expensive results as compared to standard tests for carcinogenicity done on animals, which take years to complete and are expensive to do [11, 12]. Test strains of *Salmonella typhimurium* (TA 98 and TA 100) that carry different mutation in the histidine operon are used in the Ames test for detecting reverse mutation in the histidine gene of test strains caused by mutagenic compounds.

In this study, we synthesize and characterize Schiff-base ligands and their metal complexes, carry out alkane oxidation using the *t*-butylhydroperoxide (TBHP) and/or H_2O_2 as co-catalyst and study the antimicrobial, genotoxic and electrochemical properties of the compounds.

2. Experimental

2.1. *Materials*

Metal salts, $CoCl_2 \cdot 6H_2O$, $FeCl_3 \cdot 6H_2O$ and $RuCl_3 \cdot H_2O$, H_2O_2, *t*-butylhydroperoxide (TBHP), hexane and organic solvents were purchased from commercial sources and used as received, unless otherwise noted. 2,4-dihydroxybenzaldehyde, 2,3,4-trihydroxybenzaldehyde, *o*-vanilline and 3,5-di-aminobenzoic acid were purchased from Fluka.

2.2. *Physical measurements*

Elemental analyses (C, H, N) were performed using a LECO CHNS 932 elemental analyzer. IR spectra were obtained using KBr discs (4000–400 cm^{-1}) on a Shimadzu 8300 FT-IR spectrophotometer. Electronic spectra in the 200–1100 nm range were obtained on a Shimadzu UV-160 A spectrophotometer. Magnetic measurements were carried out by the Gouy method using $Hg[Co(SCN)_4]$ as calibrant. Mass spectra of the ligands were recorded on a LC/MS APCI AGILENT 1100 MSD spectrophotometer. ^{1}H-NMR spectra were recorded on a Bruker 300 instrument. TMS was used as internal standard and deuterated DMSO-d_6 as solvent. The metal and chloride contents of the complexes were determined gravimetrically according to known procedure [13]. Thermal analyses of the complexes were performed on a Perkin-Elmer Pyris Diamond DTA/TG Thermal System under nitrogen at a heating rate of 10 °C min^{-1}. in the 298–1273 K temperature range. Gas chromatographic analyses were carried out with a HP 6189 instrument (capillary column 50 m × 0.25 mm × 0.25 μm, Carbowax 20M; integrator SP-4400; the carrier gas was helium).

Electrochemical studies were carried out with a Iviumstat Electrochemical workstation equipped with Compact Stat power connector: 5.5 mm bus female 2.1 mm inner, 5.5 mm outer diameter, recommended shaft length 12 mm center pin should be +5V ± 0.2V, max 1A. Cyclic voltammetric studies were carried out using a glassy

carbon working electrode ($A = 0.03\,cm^2$), a platinum auxiliary electrode, and a $Ag\,AgCl^{-1}$ reference electrode. The potentials were scanned from -2000 to $+2000\,mV$ employing scan rates between $50\,mV\,s^{-1}$ and $500\,mV\,s^{-1}$. The working electrode was polished intensively with aluminum oxide on a polishing cloth and degreased in methanol prior to each electrochemical measurement. The solutions were deoxygenated by passing dry nitrogen through the solution for 30 min prior to the experiments; during the experiments the flow was maintained over the solution. Digital simulations were performed using DigiSim 3.0 for Windows (BAS, Inc.). Experimental cyclic voltammograms used for the fitting process had the background subtracted and were corrected electronically for ohmic drop.

2.3. *Preparation of the ligands*

3,5-Di-aminobenzoic acid (1.52 g, 10 mmol) and respectively: 2,4-dihydroxybenzaldehyde (2.76 g, 20 mmol) or 2,3,4-trihydroxybenzaldehyde (3.08 g, 20 mmol) or *o*-vanilline (3.04 g, 20 mmol) in EtOH solutions were stirred under reflux for 2 h. The precipitated product was filtered off, washed with cold EtOH, recrystallized from hexane/EtOH (1:3 by vol) and dried in a vacuum dessiccator over P_2O_5. The purity was checked by elemental analyses and t.l.c. studies.

H_2L^1: ^{1}H-NMR: (DMSO-d_6 as solvent, δ in ppm): 13.29 (s, H, COOH), 9.87, 9.84, 8.93 (s, 3H, OH), 8.55, 8.74 (s, 2H, CH=N), 6.39–7.74 (m, Ar–H, 7H), 3.35 (s, OCH_3, 6H). Mass spectrum (LC/MS APCI): m/z 425 $[M]^+$ (25%), 426 $[M+1]$ (18%), 427 $[M+2]^{+2}$ (15%), 289 $[C_{15}H_{16}N_2O_4]^{+3}$ (100%).

H_2L^2: ^{1}H-NMR: (DMSO-d_6 as solvent, δ in ppm): 13.28 (s, COOH, 2H), 10.35, 9.92 (s, OH, 2H), 8.95, 8.77 (s, CH=N, 2H), 6.28–7.74 (m, Ar–H, 9H), 3.36 (s, OCH_3, 6H). Mass spectrum (LC/MS APCI): m/z 393 $[M]^+$ (17%), 275 $[C_{14}H_{14}N_2O_4+1]^+$ (20%), 273 $[C_{14}H_{13}N_2O_4]^+$ (100%).

H_2L^3: ^{1}H-NMR: (DMSO-d_6 as solvent, δ in ppm): 11.17 (s, COOH, 1H), 10.27 (s, OH, 2H), 9.12 (s, CH=N, 2H), 6.76–7.87 (m, Ar–H, 6H), 3.80 (s, OCH_3, 6H). Mass spectrum (LC/MS APCI): m/z 421 $[M]^+$ (10%), 311 $[C_{17}H_{15}N_2O_4]^+$ (34.1%), 312 $[C_{17}H_{16}N_2O_4]^{+2}$ (10%), 287 $[C_{15}H_{15}N_2O_4]^+$ (100%), 288 $[C_{15}H_{16}N_2O_4]^{+2}$ (17.0%), 289 $[C_{15}H_{17}N_2O_4]^{+3}$ (3.0%).

2.4. *Preparation of the complexes*

The complexes were prepared by similar methods. A solution of the metal salt (1 mmol) in anhydrous EtOH (25 cm^3) was added to a solution of the ligand (1 mmol) in absolute EtOH (20 cm^3) and the mixture was boiled under reflux for 6–7 h. At the end of the reaction, determined by t.l.c., the precipitate was filtered off, washed with distilled water and then EtOH, and dried *in vacuo*.

2.5. *Catalytic runs*

The metal complex (0.04 mmol) was dissolved in degassed acetonitrile (20 cm^3) by stirring magnetically under argon in a 100 cm^3 three-necked round bottomed flask.

Substrate (40 mmol) followed by H_2O_2/TBHP (4 mmol) were added to the above solution. An argon balloon was fitted to the flask and the resulting solution was stirred at room temperature during 24 h. The reaction products were analyzed by GC using internal standard method. Chlorobenzene for cyclohexanol and cyclohexanone was used as internal standard. The samples were analyzed twice, i.e., before and after the addition of the excess solid PPh_3. No oxidation of substrate occurred in the absence of the metal complexes.

2.6. *Ames test*

Substances including medium, buffers and S9 mix used in the Ames test were prepared as described in the study of Kayraldız *et al.* [14] with chemicals purchased from Sigma, Aldrich, or Boehringer Mannheim. Histidine deficient *Salmonella typhimurium* strains, TA 98 and TA 100 were provided by J.L. Swezey (Microbial Genomics and Bioprocessing Research Unit, North University, Illinois, USA). Dimethyl sulfoxide (DMSO) suspensions of 2-aminofluerene (2-AF) and 4-nitro-o-phenylenediamine (NPD) and also sodium azide (dissolved in distilled water) were used as positive controls. Test substance 3,5-*bis*({(1*E*)-[3-(methoxy)-2-hydroxyphenyl]methylene}amino)benzoic acid (H_2L^3) was suspended in twice distilled water with the final concentrations of 1.25, 1.00, 0.75, 0.50, and 0.25 mg/plate, for testing mutagenicity. The final concentrations, 0.62, 0.49, 0.37, 0.24, and 0.12 mg/plate of 3,5-*bis*{[(1*E*)-(2,3,4-trihydroxyphenyl)methylene]amino}benzoic acid (H_2L^1) and 0.31, 0.24, 0.18, 0.12, and 0.06 mg/plate of 3,5-*bis*{[(1*E*)-(2,4-dihydroxyphenyl)methylene]amino}benzoic acid (H_2L^2), suspended in twice distilled water, were used for mutagenicity testing. Standard procedure of plate-incorporation assay was carried out by using TA 98 and TA 100 strains for examining the frameshift mutagens and base pair substitution mutagens, respectively. Using both strains, the Ames test was performed with metabolic activation (+S9 mix) to obtain a first approximation of mammalian metabolism, and without metabolic activation (−S9 mix). The assay was carried out according to Maron and Ames [15]. TA 98 and TA 100 strains were exposed to a range of concentrations of each test substance in a soft agar overlay. The number of revertants observed in each concentration of test substances and in spontaneous control were scored. The observed differences between the test substances and control were analyzed by *t*-test. Regression and correlation tests were used for dose-responce relationships.

2.7. *Preparation of the microbial culture*

Schiff-base ligands were evaluated for their *in vitro* antibacterial activity against *Escherichia coli* ATCC 8739, *Staphylococcus aureus* Cowan 1, *Klebsiella pneumoniae* FMC 5, *Mycobacterium smegmatis* CCM 2067, *Pseudomonas aeruginosa* ATCC 27853, *Enterococcus cloacae* ATCC 13047, *Bacillus megaterium* DSM 32, *Micrococcus luteus* LA 2971 and their *in vitro* antifungal activity against *Kluyveromyces fragilis* A 230, *Rhodotorula rubra*, *Candida albicans* ATCC 1023, *Saccharomyces cerevisiae* WET136, *Trichoderma reesei* RUT by agar-well diffusion method. All the bacteria mentioned above were incubated in Nutrient Broth (NB) (Difco) at $37 \pm 0.1^{\circ}C$ for 24 h, and the yeasts were incubated in Sabouraud Dextrose Broth (SDB) (Difco) at $25 \pm 0.1^{\circ}C$ for 48 h. The bacteria and yeasts (prepared as above) were injected into petri dishes (9 cm)

in the amount of 0.01 cm^3 (10^5 cm^{-3} for the bacteria and 10^3 cm^{-3} for the fungi), 15 mL of Mueller Hinton Agar (MHA, Oxoid) and Sabouraud Dextrose Agar (SDA) (sterilized in a flask and cooled to 45–50°C) were homogenously distributed onto the sterilized petri dishes [16]. All the compounds were injected into empty sterilized antibiotic discs having a diameter of 6 mm [17] in the amount of 50 µL. The compounds to be tested were dissolved in H_2O to a final concentration of 2000 ppm and soaked in filter paper. Discs injected with complexes were located on the solid agar medium by pressing slightly. After petri dishes so obtained were placed at 4°C for 2 h, plates inoculated with fungi were incubated at 25 ± 0.1°C for 24 h. At the end of the period, inhibition zones formed on the food medium were evaluated in millimeters [16]. These studies were performed in triplicate. Gentamicin (Bioanalyse) and Nystatin (Oxoid) were used as standards.

3. Results and discussion

Three Schiff bases were synthesized from reactions between the 2,4-dihydroxybenzaldehyde, 2,3,4-trihydroxybenzaldehyde, *o*-vanilline and 3,5-diaminobenzoic acid in ethanol, 3,5-*bis*{[(1*E*)-(2,3,4-trihydroxyphenyl)methylene]amino}benzoic acid (H_2L^1), 3,5-*bis*{[(1*E*)-(2,4-dihydroxyphenyl)methylene]amino}benzoic acid (H_2L^2) and 3,5-*bis*({(1*E*)-[3-(methoxy)-2-hydroxyphenyl]methylene}amino)benzoic acid (H_2L^3). Elemental analyses (table 1) of the Schiff bases and their metal complexes agree well with the proposed composition and support 1 : 1 mole ratio of Schiff-base ligands to the metal ion. Various attempts were made to isolate single crystals, but suitable crystals were not obtained. The ligands and their metal complexes are stable solids and can be stored without decomposition at room temperature. The ligands are soluble in polar organic solvents as EtOH, MeOH, $CHCl_3$, DMSO and are partially soluble in non-polar solvents, such as hexane, heptane, toluene etc. All ligands contain –COOH on the aromatic amine ring, and their solutions are slightly acidic. All complexes of H_2L^1–H_2L^3 are mononuclear; the Co^{II} complexes are the most soluble and Ru^{III} complexes

Table 1. Physical and analytical data of the ligands and their metal complexes.

Compounds	Color	Yield	M.p. (°C)	Found (Calcd) %C	H	N	M	$^a\Lambda_M$
H_2L^1	Orange	87	>250	59.48 (59.44)	3.84 (3.80)	6.63 (6.60)	–	1.5
$[Ru(L^1)(Cl)(H_2O)]H_2O$	Brown	70	>250	42.36 (42.40)	3.10 (3.05)	4.74 (4.71)	17.04 (16.99)	7.8
$[Co(L^1)]H_2O$	Brown	64	>250	50.55 (50.52)	3.27 (3.23)	5.65 (5.61)	11.86 (11.80)	7.5
$[Fe(L^1)(Cl)(H_2O)]H_2O$	Brown	68	>250	45.93 (45.89)	3.34 (3.30)	5.14 (5.10)	10.20 (10.16)	8.0
H_2L^2	Orange	67	250	64.31 (64.28)	4.15 (4.11)	7.17 (7.14)	–	1.3
$[Ru(L^2)(Cl)(H_2O)]2H_2O$	Brown	71	>250	43.45 (43.42)	3.51 (3.47)	4.86 (4.82)	17.45 (17.40)	6.9
$[Co(L^2)]$	Green	70	>250	56.18 (56.14)	3.17 (3.14)	6.28 (6.24)	13.17 (13.12)	7.5
$[Fe(L^2)(Cl)(H_2O)]2H_2O$	Brown	90	>250	47.12 (47.08)	3.80 (3.76)	5.27 (5.23)	10.47 (10.43)	1.4
H_2L^3	Yellow	85	228	65.74 (65.71)	4.83 (4.79)	6.71 (6.66)	–	9.0
$[Ru(L^3)(Cl)(H_2O)]H_2O$	Green	65	>250	46.78 (46.75)	3.79 (3.75)	4.78 (4.74)	17.15 (17.10)	7.6
$[Co(L^3)]2H_2O$	Green	66	>250	53.85 (53.81)	4.35 (4.32)	5.50 (5.46)	11.54 (11.48)	8.1
$[Fe(L^3)(Cl)(H_2O)]H_2O$	Brown	72	>250	50.58 (50.62)	4.11 (4.06)	5.17 (5.13)	10.29 (10.23)	6.5

$^a\Omega^{-1}$ cm^2 mol^{-1}.

are the least soluble. The proposed structures of the synthesized ligands and their metal complexes are given in figure 1.

Solution conductivity (table 1) measurements show that all compounds are non-electrolytes.

To investigate the keto-enol tautomeric forms (figure 2) of the free ligands, the electronic spectra (table 2) were measured in C_6H_{14}, C_7H_8, MeOH and EtOH. In C_6H_{14} and C_7H_8, the ligands exhibit maxima in the 346–288 nm range. However, in MeOH and EtOH, new bands in the 380–350 nm range were observed. The bands in the polar solvents have been assigned to the enolimine tautomer and the nonpolar to the ketoamine tautomer of the Schiff bases.

Infrared spectral data are given in table 3. In spectra of the ligands, broad bands in the 3452–3384 cm^{-1} range are attributed to the ν(OH) vibrations. In the complexes, this band disappears confirming that oxygen coordinates to the metal ions. The ν(CH=N) vibrations of the azomethine groups of the ligands occur at 1633–1616 cm^{-1}. In the complexes, these vibrations shift, attributable to complexation of the metal to nitrogen

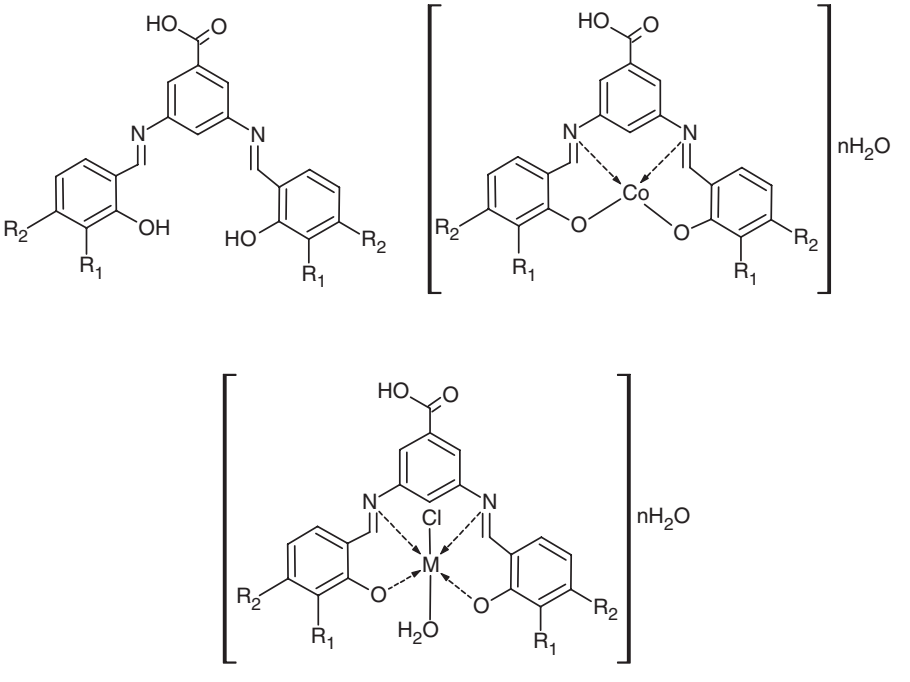

Ligand	R^1	R^2	M
H_2L^1	OH	OH	Fe^{III}, Ru^{III}
H_2L^2	H	OH	Fe^{III}, Ru^{III}
H_2L^3	OCH_3	H	Fe^{III}, Ru^{III}

Figure 1. Proposed structures of the ligands and their metal complexes.

of the azomethine. In the spectra of the complexes, the COOH groups remain free as shown by infrared bands in the region 1704–1697 cm^{-1}. The very slight blue-shifting from the free ligands may be due to rearrangement of the ligand structure, stereospecific interaction with the coordinated metal ion and the presence of coordinated water in some cases. Complexes show broad bands in the region 3340–3330 cm^{-1} along with the appearance of bands in the 985–940 cm^{-1} range (wagging modes of water) indicating coordinated water molecules [18]. New bands in the 503–478 and 430–420 cm^{-1} ranges can be attributed to ν(M–O) and ν(M–N) modes, respectively [19].

Electronic spectra of the complexes were recorded in EtOH in the 200–1100 nm range (table 4). The ligand bands in the 356–332 nm range may be assigned to n–π^*

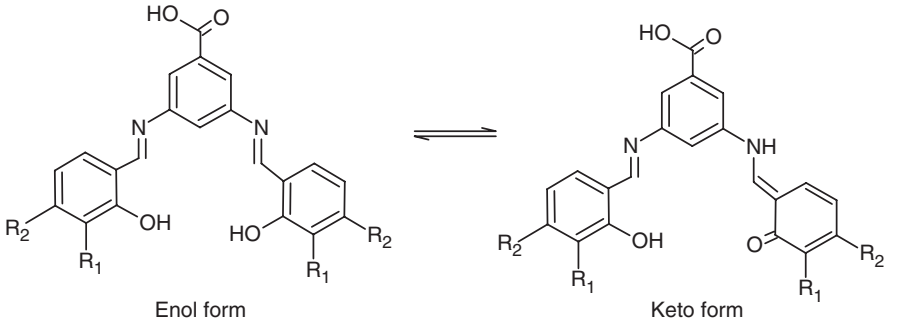

Figure 2. Keto-enol tautomeric forms of the ligands.

Table 2. Electronic spectral data in the polar and non-polar organic solvents for the keto-enol tautomeric forms (λ, nm).

Compound	EtOH	MeOH	C_7H_8	C_6H_{14}
H_2L^1	304, 332, 346, 356	301, 326, 346, 354, 380	303, 345	288, 325
H_2L^2	306, 346, 350, 356	303, 345, 351, 358	314, 345	295, 346
H_2L^3	273, 282, 302, 346, 350, 355	302, 345	319, 346	298, 346

Table 3. The infrared spectral data of the Schiff base ligands and their metal complexes (cm^{-1}) (KBr).

Compound	ν(OH)*	ν(C=O)	ν(CH=N)	ν(C–OH)	ν(M–O)	ν(M–N)
H_2L^1	3384	1699	1633	1305	–	–
$[Ru(L^1)(Cl)(H_2O)]H_2O$	3388	1701	1621	1302	497	424
$[Co(L^1)]H_2O$	3415	1704	1620	1307	478	424
$[Fe(L^1)(Cl)(H_2O)]H_2O$	3419	1701	1622	1322	503	420
H_2L^2	3420	1699	1629	1320	–	–
$[Ru(L^2)(Cl)(H_2O)]2H_2O$	3440	1699	1622	1320	497	420
$[Co(L^2)]$	–	1697	1620	1315	501	430
$[Fe(L^2)(Cl)(H_2O)]2H_2O$	3419	1697	1618	1317	491	420
H_2L^3	3452	1703	1616	1344	–	–
$[Ru(L^3)(Cl)(H_2O)]H_2O$	3440	1698	1610	1322	493	430
$[Co(L^3)]2H_2O$	3419	1702	1630	1310	503	430
$[Fe(L^3)(Cl)(H_2O)]H_2O$	3423	1701	1647	1305	499	420

*$\nu(H_2O)$ for the complexes containing water molecule(s).

transitions, while those in the 306–273 nm range can be attributed to the π–π^* and π–δ^* transitions. The Co(II) complexes show d-d transitions in the 675–640 nm range and bands in the 457–377 nm range can be assigned to $d_\pi(Co) \rightarrow \pi^*$(ligand) charge transfer transitions [20]. Absorption bands appearing at energies higher than ~400 nm are associated with ligand transitions.

In Ru^{III} complexes, the bands in the 581–550 nm range are assigned to d-d transitions, bands in the 476–356 nm range to the $d_\pi(Ru) \rightarrow \pi^*(L)$ (symmetric) and $d_\pi(Ru^{III}) \rightarrow \pi^*(L)$ (antisymmetric) MLCT transitions. The band near 350 nm may be due to the $d_\pi(Ru) \rightarrow L$ (MLCT) transition. The higher energy bands in the UV region are of intra-ligand π–π^* type or charge-transfer transitions.

The magnetic moments of the complexes at room temperature (298 K) are given in table 4. Tetrahedral cobalt(II) complexes have magnetic moments in the 4.21–4.38 B.M. range [21], higher than the spin-only value. Tetrahedral complexes are supported by the visible spectra in the 675–640 nm range assignable to the $^4A_2 \rightarrow {}^4T_1(P)$ transition in tetrahedral geometry. The magnetic moment data for the Ru^{III} complexes are in the 1.75–1.82 B.M. range, corresponding to one unpaired electron with low spin $t^5{}_{2g}$ configuration for Ru^{III} in an octahedral environment. The Fe^{III} complexes show higher magnetic moments than the spin-only values for one electron ($\mu_{eff} = 1.73$ B.M.) in the 1.74–1.82 B.M. range consistent with octahedral geometry.

^{1}H-NMR spectra of the ligands (Supplementary material) indicate one signal for the azomethine protons. Broad bands in the 13.28–13.32 ppm range are assigned to the COOH groups, and broad singlets in the 10.35–9.11 ppm range to phenolic hydroxyl. The singlet due to azomethine (–CH=N–) are in the δ 8.65–9.12 ppm range. Aromatic ring protons are shown in the 8.95–8.55 ppm and 6.28–7.75 ppm ranges. The very strong singlets in the 3.84–3.36 ppm range are attributed to $-OCH_3$.

Mass spectral data of the ligands H_2L^1–H_2L^3 are given in the experimental section. The spectrum of the $[Ru(L^3)(Cl)(H_2O)]H_2O$ complex is shown in Supplementary data. Mass spectra of the Schiff-base ligands indicate parent ions $[M]^+$ at *m/e* 425, 393, 421 for the ligands H_2L^1, H_2L^2 and H_2L^3, respectively. The peaks at *m/e* 289, 273 and 288 have the highest intensity for the ligands, attributed to $[C_{15}H_{16}N_2O_4]^+$, $[C_{14}H_{13}N_2O_4]^+$ and $[C_{15}H_{15}N_2O_4]^+$ ions. In the complexes, molecular ion peaks (M^+) are in the *m/z* 449–595 range.

Thermal properties of the complexes in the 298–1273 K range reveal adsorbed or coordinated water and chloride, consistent with the analytical and spectroscopic data. Dehydration in the 323–373 K range indicates water in the outer sphere. For Co^{II}, CoO forms in the 573–917 K range which is oxidized to Co_3O_4 (in the 919–965 K range), the

Table 4. The electronic (in EtOH) and magnetic data (at room temperature) of the metal complexes.

Compound	μ_{eff} (B.M.)	λ_{max} (nm)
$[Ru(L^1)(Cl)(H_2O)]H_2O$	1.82	302, 346, 350, 359, 470, 532
$[Co(L^1)]H_2O$	4.24	348, 379, 675
$[Fe(L^1)(Cl)(H_2O)]H_2O$	1.82	302, 347, 367, 468, 560
$[Ru(L^2)(Cl)(H_2O)]2H_2O$	1.75	275, 280, 307, 316, 430, 523
$[Co(L^2)]$	4.38	285, 305, 350, 373, 640
$[Fe(L^2)(Cl)(H_2O)]2H_2O$	1.74	295, 346, 361, 474, 536
$[Ru(L^3)(Cl)(H_2O)]H_2O$	1.80	277, 333, 346, 356, 476, 540
$[Co(L^3)]2H_2O$	4.21	289, 346, 379, 660
$[Fe(L^3)(Cl)(H_2O)]H_2O$	1.79	302, 346, 385, 472, 550

final product of the complex decomposition. The results indicate the following thermal decompositions of the complexes:

$$[Fe(L^m)_n(Cl)(H_2O)] \cdot xH_2O \rightarrow [Fe(L^m)_n(Cl)(H_2O)] \rightarrow [Fe(L^m)_n] \rightarrow Fe_2O_3$$
$$[Co(L^m)_n] \cdot xH_2O \rightarrow [Co(L^m)_n] \rightarrow CoO \rightarrow Co_3O_4$$
$$[Ru(L^m)_n(Cl)(H_2O)] \cdot xH_2O \rightarrow [Ru(L^m)_n(Cl)(H_2O)] \rightarrow [Ru(L^m)_n] \rightarrow Ru_2O_3$$

3.1. *Catalytic oxidation of cyclohexane*

The catalytic activity of the complexes for the oxidation of cyclohexane with hydrogen peroxide/TBHP under argon in acetonitrile was examined for 24 h. The samples were analyzed twice, i.e., before and after the addition of the excess PPh_3, a method which allows detection of alkyl/hydroperoxides and to measure the real concentrations of the products [24]. The obtained data are summarized in table 5. The oxidation of cyclohexane proceeds with an induction period (a few minutes; the induction period being longer at 0°C) during which the color of the solution changes from brown and/or green to pale. The subsequent reaction gives oxygenated products, and the reaction solution gradually becomes almost colorless. The reactions were quenched by addition of triphenylphosphine, and GC analysis gave concentrations of cyclohexanol and cyclohexanone as the reaction products. A comparison of alcohol and ketone concentrations (measured by GC) before and after the addition of PPh_3. The solution not treated with PPh_3 contains alkyl hydroperoxide, ROOH, which decomposes in GC to produce ROH and R=O compounds.

$$C_6H_{12} + H_2O_2 \text{ or } (t - C_4H_9O_2H) + \frac{1}{2}O_2 \rightarrow C_6H_{11}OOH \text{ or } (C_6H_{11}OOC_4H_9) + H_2O$$
$$2C_6H_{11}OOH \text{ or } (C_6H_{11}OOC_4H_9) \rightarrow C_6H_{11}OH + C_6H_{10}O$$

The total concentration of oxygenates (cyclohexanol and cyclohexanone) determined before treatment with PPh_3 is much lower than the concentration after reduction with PPh_3. This can be understood, assuming either partial decomposition of ROOH in GC to produce ring-opened products (e.g., adipic acid) and/or the appearance of ROOH as a separate peak on the chromatogram (in some cases we were able to detect such peaks).

Table 5. Oxidation of cyclohexane catalyzed under argon (24 h).

Complex	TBHP/H_2O_2 (mmol)	Yield (%) CyOL	CyONE
$[Ru(L^1)(Cl)(H_2O)]H_2O$	4	20	37
$[Co(L^1)]H_2O$	4	13	30
$[Fe(L^1)(Cl)(H_2O)]H_2O$	4	25	45
$[Ru(L^2)(Cl)(H_2O)]2H_2O$	4	18	33
$[Co(L^2)]$	4	9	29
$[Fe(L^2)(Cl)(H_2O)]2H_2O$	4	23	42
$[Ru(L^3)(Cl)(H_2O)]H_2O$	4	19	35
$[Co(L^3)]2H_2O$	4	9	27
$[Fe(L^3)(Cl)(H_2O)]H_2O$	4	24	41

The most efficient catalysts are the Fe^{III} complexes, which is unusual because, in general, the cobalt(II) complexes have high activity for alkane oxidation reactions.

The oxidation products occurs with auto-acceleration, apparently due to gradual destruction of the complexes to more catalytically efficient species.

3.2. *Electrochemistry*

The redox properties of the Ru^{III} complexes (1×10^{-3} M) were investigated in DMF (in nitrogen atmosphere) by cyclic voltammetry and are metal centered (table 6). Cyclic voltammograms of all the complexes are recorded at 50 and 500 mVs^{-1} scan rates. Representative cyclic votammograms of $[Ru(L^1)(Cl)(H_2O)] \cdot H_2O$ and $[Ru(L^2)(Cl)(H_2O)] \cdot 2H_2O$ are shown in figure 3a and 3b. The number of electrons transferred in the electrode reaction for a reversible couple can be determined from the separation between the peak potential.

$$\Delta E_p = E_{pa} - E_{pc} = \frac{0.0591}{n}$$

where E_{pa}, E_{pc}, and n are anodic potential, cathodic potential and the number of electrons transferred, respectively. Thus, a one-electron process exhibits a ΔE_p approximately 0.059 V at 50 mVs^{-1}, the Ru^{III} complexes showed well-defined waves in the ($E_{1/2}$) −0.95 to +0.45 V (Ru^{IV}/Ru^{III}) and (Ru^{III}/Ru^{II}) range *versus* Ag/AgCl. At 0.10 and −0.51 V, the ratio ip/sr (ip = peak current; sr = scan rate) is one, indicating that the electron transfer is reversible. The electron donating group (–OH) substituent on the phenyl ring of the Schiff base favored oxidation of Ru^{III} to Ru^{IV} [25]. The electrochemistry of these complexes in DMF consists of a well-defined Ru(III/II) oxidation couple, the position of which is highly dependent upon the substituent. The electron-donating methoxy and hydroxy substituents shift the $Ru^{III/II}$ oxidation to more positive potentials.

$$[Ru^{III}(X)Cl(H_2O)] \rightleftharpoons [Ru^{IV}Cl(H_2O)(X)]^+ + e^-$$

Cyclic voltammograms of the Co^{II} complexes (1×10^{-3} M) exhibit reversible oxidation and reduction peaks at 50 and 500 mVs^{-1}. At 50 mVs^{-1}, the $[Co(L^1)] \cdot H_2O$ and $[Co(L^3)] \cdot 2H_2O$ complexes show reversible oxidation peaks at −1.88 and 0.35 V, respectively. These peaks change to −0.99 and −0.66 V for oxidation and −0.52 and −0.44 V for reduction processes, respectively. One quasi-reversible redox couple is a common feature of the cyclic voltammograms of the Co^{II} complexes. $Co(L^2)$ shows an irreversible peak at −0.25 V (scan rate: 50 mVs^{-1}). At 500 mVs^{-1}, the complex shows a quasi-reversible peak at 0.77 V assigned to the $Co^{II/I}$ couple.

$$[Co^{II}(L^{1-3})] \underset{-e^-}{\overset{+e^-}{\rightleftharpoons}} [Co^{I}(L^{1-3})]$$

Cyclic voltammograms of Fe^{III} complexes at scan rate 50 mVs^{-1} have peaks in the −1.88–(−0.05) V and 0.30–(−0.18) V range for anodic and cathodic potentials, respectively. At scan rate 500 mVs^{-1}, these peaks shift to more positive regions. By introduction of an electron-withdrawing COOH group, the redox potential shifts to more positive values.

Table 6. Electrochemical data of all the compounds.

Compounds	*E_{pa} (V)	*E_{pc} (V)	$E_{1/2}$ (mV)	ΔE_p(mV)	**E_{pa} (V)	**E_{pc} (V)	$E_{1/2}$ (mV)	ΔE_p (mV)
$[Ru(L^1)(Cl)(H_2O)]H_2O$	0.09	0.10, 0.81	450	−720	0.29, −0.77	1.00	645, 115	−710
$[Co(L^1)]H_2O$	−1.88, −0.39	1.46	−210, 535	−3340	−0.99, −0.59	−0.52, −0.10	−470, −245	−1510
$[Fe(L^1)(Cl)(H_2O)]H_2O$	−1.88	0.13	−875	−2010	−0.48	−1.49	−985	1010
$[Ru(L^2)(Cl)(H_2O)]2H_2O$	−1.01, −0.51	−0.60, 0.74	−805	−410	−0.22	1.41	595	−1630
$[Co(L^2)]$	−0.25, 0.32	1.39, −0.07	570, 130	−1640	−0.42, 0.77	−0.53, 1.48	−55, 1125	110
$[Fe(L^2)(Cl)(H_2O)]2H_2O$	−1.88	−0.18	1030	−1700	−1.32	0.59	−365	−1910
$[Ru(L^3)(Cl)(H_2O)]H_2O$	−1.33	−0.57	−950	−760	−0.22	1.30	540	−1520
$[Co(L^3)]2H_2O$	−1.88, 0.35	−0.59, −0.38	1235, −15	−1290	−0.66	−0.44	−550	−220
$[Fe(L^3)(Cl)(H_2O)]H_2O$	−0.05	0.30	125	−350	−0.47	0.67	100	−1140

*scan rate: 50 mV/s; **scan rate: 500 mV/s. Supporting electrolyte: tetrabutylammonium hexafluorophosphate (0.1 M); concentration of the complex: 10^{-3} M. All the potentials are referenced to Ag/AgCl; where E_{pa} and E_{pc} are anodic and cathodic potentials, respectively. $E_{1/2} = 0.5 \times (E_{pa} + E_{pc})$, $\Delta E_p = E_{pa} - E_{pc}$.

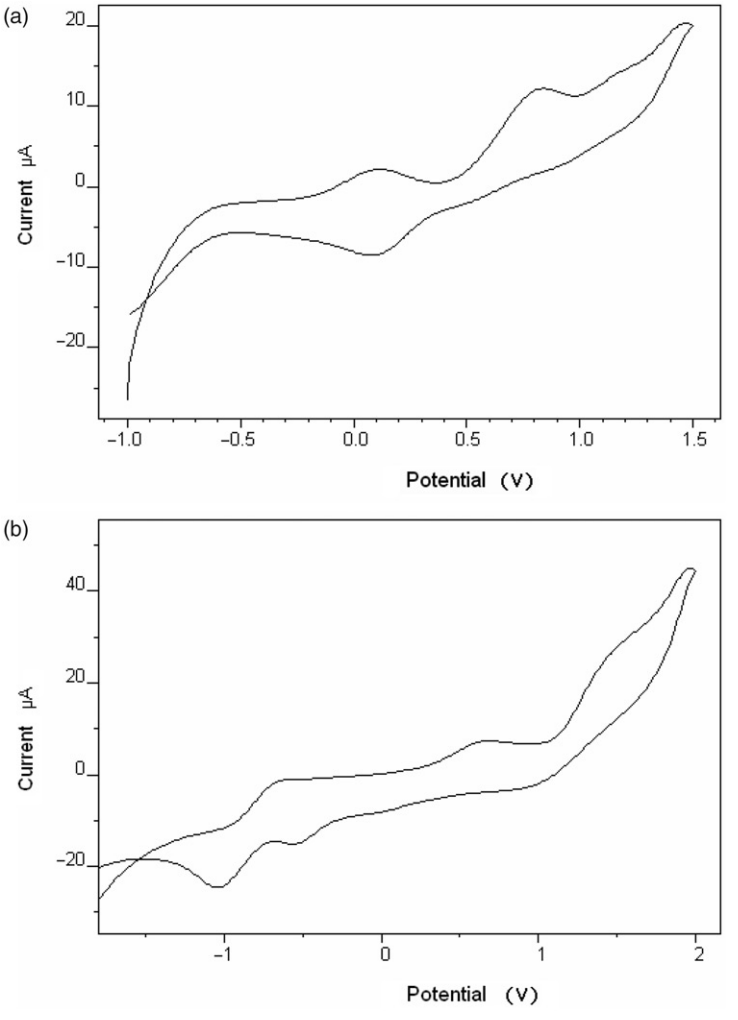

Figure 3. The cyclic voltammograms of $[Ru(L^1)(Cl)(H_2O)]H_2O$ (a) and $[Ru(L^2)(Cl)(H_2O)]2H_2O$ (b) complexes in DMF solution (0.1 M TBAHFP as supporting electrolyte).

3.3. *Ames test*

The data from the Ames mutagenicity test are given in table 7. The 3,5-*bis*{[(1*E*)-(2,3,4-trihydroxyphenyl)methylene]amino}benzoic acid (H_2L^1), 3,5-*bis*{[(1*E*)-(2,4-dihydroxyphenyl)methylene]amino}benzoic acid (H_2L^2) and 3,5-*bis*({(1*E*)-[3-(methoxy)-2-hydroxyphenyl]methylene}amino)benzoic acid (H_2L^3) were mutagenic on *S. Typhimurium* TA 98 in the presence and absence of S9 mix. The mutagenic activity of H_2L^2 on the TA 100 strain increased with increasing dose in the absence of S9 mix (shown in Supplementary data). The ligands H_2L^1 and H_2L^2 showed mutagenic activity on TA 100 with and without S9 mix. In the absence of S9 mix, the mutagenic activity of the ligand H_2L^2 on the TA 98 or TA 100 strain was dose-dependent. The ligand H_2L^3 was not mutagenic for TA 100 in the presence or absence of S9 mix, as shown in table 7. All tested ligands and their various

Table 7. The mutagenicity of test substances in *Salmonella typhimurium* TA 98 and TA 100 strains in the absence or presence of S9 mix.

		TA 98		TA100	
Test substances	Conc. mg/plate	−S9	+S9	−S9	+S9
Spontaneous control	–	15.8 ± 3.2	23.6 ± 4.5	95.4 ± 15.9	107.0 ± 10.3
NPD		3073.4 ± 310.3			
2-AF			809.0 ± 46.0		1838.4 ± 337.4
SA				815.4 ± 88.4	
H_2L^1	0.62	162.8 ± 28.2**	166.7 ± 45.2*	30.2 ± 7.4**	59.5 ± 11.2*
	0.49	171.5 ± 49.2*	86.0 ± 8.6*	27.0 ± 5.5***	48.4 ± 16.6*
	0.37	139.0 ± 10.3**	130.3 ± 24.3*	26.8 ± 8.8**	23.6 ± 8.2**
	0.24	62.4 ± 17.2*	72.5 ± 19.3	21.4 ± 8.1**	30.0 ± 7.8**
	0.12	34.4 ± 6.3*	93.3 ± 7.7**	11.8 ± 4.1***	7.4 ± 1.9***
H_2L^2	0.31	68.8 ± 7.1**	96.8 ± 15.3**	302.8 ± 38.3**	441.4 ± 53.1
	0.24	65.4 ± 23.0	86.2 ± 20.0	248.4 ± 59.6	399.6 ± 44.7*
	0.18	61.2 ± 7.5**	87.8 ± 12.9**	190.0 ± 49.1	190.8 ± 54.5
	0.12	40.4 ± 10.8	109.0 ± 34.2	131.2 ± 29.1	357.5 ± 50.5
	0.06	14.5 ± 3.5	87.5 ± 9.5**	118.6 ± 6.7	178.3 ± 4.0**
H_2L^3	1.25	4014.0 ± 472.0**	4577.0 ± 825.0*	120.6 ± 13.6	76.8 ± 13.0
	1	3495.6 ± 205.5***	2794.5 ± 865.7*	115.2 ± 13.5	101.2 ± 12.5
	0.75	3193.2 ± 606.5**	3276.0 ± 861.1*	95.4 ± 16.7	111.8 ± 47.2
	0.50	1776.2 ± 219.1**	1522.6 ± 326.9*	96.6 ± 23.0	86.0 ± 6.4
	0.25	1877.4 ± 223.7**	1642.3 ± 320.2*	97.0 ± 15.2	75.2 ± 30.7

*$P < 0.05$; **$P < 0.01$; ***$P < 0.001$.
NPD: 4-nitro-*o*-phenylenediamine, **2-AF**: 2-aminofluorene, **SA**: sodium azid.

metabolites induced frameshift mutation (TA 98); in addition, H_2L^1 and H_2L^2 and their metabolites induced base-pair substitutions (TA 100).

3.4. *Biological activity*

The antibacterial and antifungal activity of the three new compounds were tested by the disc diffusion method. The antibacterial and antifungal activities of the new compounds against the bacteria *Escherichia coli*, *Staphylococcus aureus*, *Klebsiella pneumoniae*, *Mycobacterium smegmatis*, *Pseudomonas aeruginosa*, *Enterococcus cloacae*, *Bacillus megaterium*, *Micrococcus luteus*, and the fungi *Kluyveromyces fragilis*, *Rhodotorula rubra*, *Candida albicans*, *Saccharomyces cerevisiae*, *Trichoderma reesei*, are presented in table 8. The results show that H_2L^1 exhibits moderate activity against all tested bacteria and *Candida albicans* fungus. H_2L^1 showed the highest effect against *Kluyveromyces fragilis* and *Rhodotorula rubra*, but no activity against *Saccharomyces cerevisiae* and *Trichoderma reesei* fungi. H_2L^2 exhibits moderate activity against *Klebsiella pneumoniae*, *Pseudomonas aeruginosa* and *Micrococcus luteus* and H_2L^2 higher effect against *Bacillus megaterium* and *Rhodotorula rubra* than the other microorganisms in this study. H_2L^2 showed the highest effect against *Candida albicans*, *Saccharomyces cerevisiae* and *Trichoderma reesei*, but no activity against the other microorganisms. H_2L^3 exhibits moderate activity against *Staphylococcus aureus*, *Klebsiella pneumoniae* and *Mycobacterium smegmatis*, higher effect against *Candida albicans* than the other microorganisms and the highest effect against *Rhodotorula rubra* and *Saccharomyces*

Table 8. Antimicrobial effects of the ligands.

	Bacteria inhibition zone (mm)								Fungi inhibition zone (mm)				
Ligand	*Escherichia coli*	*Staphylococcus aureus*	*Klebsiella pneumoniae*	*Mycobacterium smegmatis*	*Pseudomonas aeruginosa*	*Enterococcus cloacae*	*Bacillus megaterium*	*Micrococcus luteus*	*Kluyveromyces fragilis*	*Rhodotorula rubra*	*Candida albicans*	*Saccharomyces cerevisiae*	*Trichoderma reesei*
H_2L^1	9	8	7	7	9	9	9	8	46	18	9	0	0
H_2L^2	0	0	9	0	7	0	10	7	0	10	15	12	12
H_2L^3	0	8	9	7	0	0	0	0	0	15	10	12	0

Conc. of compounds is 2000 ppm, 50 μL/disc; including diameter of disc (6 mm).

cerevisiae, but no activity against the other microorganisms. The variation in the activity of different metal complexes against different microorganisms depends on either the impermeability of the cells or the differences in ribosomes in microbial cells [17].

Supporting information

Supplementary data associated with this article can be found in the online version of this journal. This material is available free of charge on the web at http://www.informaworld.com/terms-and-conditions-of-access.pdf.

Acknowledgements

This work was supported by the University Research Foundation (Project No: 2004/7–5); therefore, we thank our research institute.

References

[1] A.D. Garnovskii, A.L. Nivorozhkin, V.I. Minkin. *Coord. Chem. Rev.*, **126**, 1 (1993).
[2] X.-G. Zhou, J.-S. Huang, P.-H. Ko, K.-K. Cheung, C.-M. Che. *J. Chem. Soc., Dalton Trans.*, 3303 (1999).
[3] A.E. Shilov, G.B. Shul'pin. *Chem. Rev.*, **97**, 2879 (1997).
[4] C. Kim, K. Chen, L. Jr. Que. *J. Am. Chem. Soc.*, **119**, 5964 (1997).
[5] M. Harthmann, S. Ernst. *Angew. Chem. Int. Ed.*, **39**, 888 (2000).
[6] S. Itoh, M. Taki, H. Nako, P.L. Holland, W.B. Toman, L. Lr. Que, S. Fukuzumi. *Angew. Chem. Int. Ed.*, **39**, 398 (2000).
[7] H. Temel, U. Cakir, V. Tolan, B. Otludiil, H.I. Ugras. *J. Coord. Chem.*, **57**, 571 (2004).
[8] H. Moawad, W.M. El-Rahim, M. Khalafallah. *J. Basic Microbiol.*, **43**, 218 (2003).
[9] I. Rodeiro, L. Cancino, J.E. Gonzalez, J. Morffi, G. Garrido, R.M. Gonzalez, A. Nunez, R. Delgado. *Food Chem. Toxicol.*, **44**, 1707 (2006).
[10] B.N. Ames, J. Mc Cann, E. Yamasaki. *Mutation Research*, **31**, 347 (1975).
[11] K. Mortelmans, E. Zeiger. *Mutation Research*, **455**, 29 (2000).
[12] D. Krewski, B.G. Leroux, S.R. Bleuer, L.H. Broekhoven. *Biometrics*, **49**, 499 (1993).
[13] A.I. Vogel. *Test Book of Practical Organic Chemistry*, 5th Edn, pp. 464–468, Longman, London (1989).
[14] A. Kayraldız, F.F. Kaya, S. Canımoğlu, E. Rencüzoğulları. *Ann. Microbiol.*, **56**, 129 (2006).
[15] D.M. Maron, B.N. Ames. *Mutation Research*, **113**, 173 (1983).
[16] C.H. Collins, P.M. Lyne, J.M. Grange. *Microbiological Methods*, 6th Edn, pp. 157–168 (1989).
[17] S.K. Sengupta, O.P. Pandey, B.K. Srivastava, V.K. Sharma. *Tran. Met. Chem.*, **23**, 349 (1998).
[18] M. Tümer, N. Deligönül, A. Gölcü, E. Akgün, M. Dolaz. *Tran. Met. Chem.*, **31**, 1 (2006).
[19] M. Tümer. *Synthesis and Reactivity in Inorganic and Metal-Organic Chemistry*, **30**, 1139 (2000).
[20] H. Demirelli, M. Tümer, A. Gölcü. *Bull. Chem. Soc. Jpn*, **79**, 867 (2006).
[21] A. Gölcü, M. Tümer, H. Demirelli, R.A. Wheatley. *Inorg. Chim. Acta*, **358**, 1785 (2005).
[22] M. Tümer, D. Ekinci, F. Tümer, A. Bulut. *Spectrochim. Acta Part: A*, **67**, 916 (2007).
[23] M. Tümer. *J. Coord. Chem.*, **60**, 2051 (2007).
[24] G.B. Shul'pin, A.N. Druzhinina. *React. Kinet. Catal. Lett.*, **47**, 207 (1992).
[25] M.S. El-Shahawi, A.F. Shoair. *Spectrochim. Acta A*, **60**, 121 (2004).